BJR

https://doi.org/10.1259/bjr.20180978

Received: 19 November 2018 | Revised: 19 April 2019 | Accepted: 19 May 2019

Cite this article as:
Cheng Q, Ye S, Fu C, Zhou J, He X, Miao H, et al. Quantitative evaluation of computed and voxelwise computed diffusion-weighted imaging in breast cancer. *Br J Radiol* 2019; **92**: 20180978.

FULL PAPER

Quantitative evaluation of computed and voxelwise computed diffusion-weighted imaging in breast cancer

QINGYUAN CHENG, SHUXIN YE, CHUQI FU, JIEJIE ZHOU, XIAXIA HE, HAIWEI MIAO, NINA XU and MEIHAO WANG

Department of Radiology, First Affiliated Hospital of Wenzhou Medical University, Wenzhou, China

Address correspondence to: Mr Meihao Wang
E-mail: *wzwmh@wmu.edu.cn*

Objectives: To assess the value of computed diffusion-weighted imaging (cDWI) and voxelwise computed diffusion-weighted imaging (vcDWI) in breast cancer.
Methods: This retrospective study involved 130 patients (age range, 25–70 years; mean age ± standard deviation, 48.6 ± 10.5 years) with 130 malignant lesions, who underwent MRI examinations, including a DWI sequence, prior to needle biopsy or surgery. cDWIs with higher *b*-values of 1500, 2000, 2500, 3000, 3500, and 4000 s/mm^2, and vcDWI were generated from measured (m) DWI with two lower *b*-values of 0/600, 0/800, or 0/1000 s/mm^2. The signal-to-noise ratio (SNR) and contrast ratio (CR) of all image sets were computed and compared among different DWIs by two experienced radiologists independently. To better compare the CR with the SNR, the CR value was multiplied by 100 (CR100).
Results: The CR of vcDWI, and cDWIs, except for $cDWI_{1000}$, differed significantly from that of measured diffusion-weighted imaging (mDWI) ($cDWI_{1000}$: CR = 0.4904, p = 0.394; $cDWI_{1500}$: CR = 0.5503, p = 0.006; $cDWI_{2000}$: CR = 0.5889, p < 0.001; $cDWI_{2500}$: CR = 0.6109, p < 0.001; $cDWI_{3000}$: mean = 0.6214, p < 0.001; $cDWI_{3500}$: CR = 0.6245, p < 0.001; $cDWI_{4000}$: CR = 0.6228, p < 0.001). The vcDWI provided the highest CR, while the CRs of all cDWI image sets improved with increased *b*-values. The SNR of neither $cDWI_{1000}$ nor vcDWI differed significantly from that of mDWI, but the mean SNRs of the remaining cDWIs were significantly lower than that of mDWI. The SNRs of cDWIs declined with increasing *b*-values, and the initial decrease at low *b*-values was steeper than the gradual attenuation at higher *b*-values; the CR_{100} rose gradually, and the two converged on the *b*-value interval of 1500–2000 s/mm^2 .
Conclusions: The highest CR was achieved with vcDWI; this could be a promising approach easier detection of breast cancer.
Advances in knowledge: This study comprehensively compared and evaluated the value of the emerging post-processing DWI techniques (including a set of cDWIs and vcDWI) in breast cancer.

INTRODUCTION

Increasingly, the limitations of screening for breast cancer by mammography and ultrasound are being recognized,[1,2] especially for Asian females, who have much denser mammary glands than European females. Therefore, advanced MRI plays a significant role in breast examinations. Mainly due to its high sensitivity. While diffusion-weighted MRI (DWI), as a functional sequence, provides information on the local microstructural characteristics of the diffusivity of water molecules in tissues,[3] allowing indirect assessment of tissue microstructure and cellular density.[4] DWI used in conjunction with dynamic contrast-enhanced (DCE) has been shown to improve the specificity of breast cancer detection, but not alone, DWI shows advantages in qualitative and quantitative analysis, lesion detection and differentiation.[5] It has been reported that DWI can provide valuable additional information for detection, localization, and characterization of malignant lesions in a variety of organs, and the assessment of treatment response.[6–10] This functional MRI sequence allowed better detection and diagnosis of breast cancer in terms of contrast between cancerous tissue (more diffusion-restricted) and normal glandular tissue (less diffusion-restricted). The contrast is controlled by the diffusion-sensitizing gradient, represented by *b*-values.[11] Conventional DWI of the breast is obtained with *b*-values of 600–1000 s/mm^2, which is not sufficiently high to optimize contrast between breast lesions and background tissue.[12,13] The lack of suppression of signal within the normal glandular tissue at these *b*-values obscures the potential hyperintensity within tumors.[14] However, using higher *b*-values may result in a poor signal-to-noise ratio (SNR), eddy current distortions, and a long scanning time, due to the larger diffusion-sensitizing gradients.[12,15] Therefore, various DWI post-processing techniques have been proposed to resolve the noise or image quality issues, to maintain or enhance the contrast between the lesion and

normal tissue. These include computed diffusion-weighted imaging (cDWI) and apparent diffusion coefficient (ADC)-dependent voxelwise computed diffusion-weighted imaging (vcDWI).[15,16]

The usefulness of cDWI and vcDWI for detection of physical lesions has been demonstrated in a few reports. For instance, Marnix et al[17] reported on high *b*-value cDWI of the prostate. Other studies have investigated the value of cDWI in imaging of the prostate and abdomen.[12,14,17–21] These reports state that cDWI with high *b*-values can provide good image quality, high contrast-to-noise ratios (CRs), and increase lesion conspicuity. Gatidis et al[22] performed phantom studies to evaluate ADC-dependent vcDWI, and demonstrated that vcDWI markedly increased the contrast and SNR of images by effectively reducing T_2 shine-through effects.

Nevertheless, to date, no study has comprehensively compared or evaluated the value of these new methods in breast cancer. This study therefore explored the value of the different post-processing DWI techniques (including a set of cDWIs and vcDWI) in breast cancer. We investigated and compared the CRs between tumor-suspected lesions and normal-appearing tissue, and the SNR in images among post-processed DWI and conventional DWI scans, and obtained the optimal *b*-value range of cDWI for breast cancer.

METHODS AND MATERIALS

Patients

Our study was approved by the relevant institutional review board, and the need to obtain informed patient consent was waived due to the retrospective nature of the study. A total of 149 patients with suspicious lesions found in ultrasound or mammography, had undergone preoperative 3.0 T MRI examination as well as pathology examination (based on ultrasound-guided core needle biopsy or surgical specimens) were identified. The MRI examinations were performed within the 7th⁻14th day of the menstrual cycle. 16 patients were excluded due to artifacts (*n* = 16) or undetectable lesion on DWI (*n* = 3). For the remaining 130 patients (age range, 25–70 years; mean age ± standard deviation, 48.6 ± 10.5 years), the pathological diagnosis included 97 cases of invasive breast carcinoma and 33 cases of ductal carcinoma *in situ* (DCIS). The 97 cases of invasive breast carcinoma included 65 cases of invasive ductal carcinoma (IDC), 23 cases of invasive lobular carcinoma (ILC), 5 cases of mucinous adenocarcinoma, and 4 case of medullary carcinoma; while the 33 DCIS cases included 18 cases of DCIS with micro-invasion (Table 1).

Table 1. Histological classification of breast cancer

Type	Subtype	N
Invasive breast carcinoma	IDC	65
	ILC	23
	Mucinous adenocarcinoma	5
	Medullary carcinoma	4
DCIS	Pure DCIS	15
	DCIS with microinvasion	18

DCIS, ductal carcinoma *insitu*; IDC, invasive ductal carcinoma; ILC, invasive lobular carcinoma; (N: Number).

MRI PROTOCOL

All patients underwent MRI on a 3T scanner (GE SIGNA EXCITE 3.0T ; GE Medical Systems, 3200N, Grandview Blvd, Waukesha, WI 53188, United states of America) using an 8-channel breast coil. For pre-menopausal females, the examination was performed within the 7th–14th day of menstrual cycle. The protocol consisted of T_2 weighted imaging (T_2WI) with fat suppression [repetition time (TR) 8200 ms; echo time (TE) 36 ms; FA 90°; slice thickness/gap 4.0/1.0 mm; field of view (FOV) 32 × 32 cm^2; matrix size 128 × 128], T_1 weighted imaging (T_1WI) with dual-echo chemical-shift imaging (TR 380 ms; TE 2 ms; FA 90°; slice thickness/gap 4.0/1.0 mm; FOV 32 × 32 cm^2; matrix size 128 × 128). Axial DWI was performed by using single-shot echoplanar imaging (EPI) sequence (TR 5300 ms; TE 60 ms; FA 90°; slice thickness/gap 4.0/1.0 mm; FOV 32 × 32 cm^2; matrix size 128 × 128; two *b*-values: 0/600 (*n* = 13), 0/800 (*n* = 9) or 0/1000 (*n* = 108) s/mm^2; spectral adiabatic inversion recovery fat suppression). The TE was kept at 60 ms for all three pairs of *b*-values, which was chosen to be as short as possible to improve SNR, and kept the same to minimize its impact affecting the image quality and the reading. The DCE scan was acquired by the volume imaging for breast assessment (VIBRANT) (TR 5 ms; TE 2 ms; FA 10°; slice thickness 1.2 mm; FOV 34 × 34 cm^2; matrix size 416 × 416). The contrast agent, 0.1 mmol/kg gadopantatedimeglumine (Magnevist; Bayer Schering Pharma), was intravenously injected. The DCE series consisted of six phases: one before and five after contrast injection. The total scanning time for one patient was 18 min and 32 s.

CDWI METHOD

The signal intensity on DWI exponentially attenuates with b-values based on a measured ADC value.[18] cDWI is synthetic image generated by extrapolating the decaying signal measured in the original DWI.[14]

ADC maps and cDWIs with different *b*-values were calculated using an in-house prepared MATLAB script (MATLAB and Statistics Toolbox Release 2015b, MathWorks, Natick, MA). The ADC was calculated on the basis of a monoexponential model with a formula based on two or more measured DWI signals.[14]

$$ADC = ln(-S1/S2)/(b1 - b2) \quad (1)$$

where S_1 is the signal intensity (SI) for b = b_1 and S_2 is the SI for b = b_2. ADC maps were constructed with the same equation on the basis of a voxelwise calculation. With a known ADC and SI S_0 at $b = 0$, the computed DWI signal for $b = b_x$ was then obtained with the equation[14]:

$$S_x = S_0\, exp\,[-(b_x - b_0)ADC] \quad (2)$$

Seven cDWI series were created by using the following *b*-values: 1000, 1500, 2000, 2500, 3000, 3500, and 4000 s/mm^2(cDWI$_{1000}$, cDWI$_{1500}$, cDWI$_{2000}$, cDWI$_{2500}$, cDWI$_{3000}$, cDWI$_{3500}$, and cDWI$_{4000}$, respectively).

VCDWI METHOD

For the above cDWI calculation method, all voxels of a cDWI image used one *b*-value; the SI of the cDWI images decreased as the *b*-value increased, but the restricted tissue attenuated relatively more slowly than did the non-restricted tissue.

The degree of diffusion in the different tissues varied. Recently, Gatidis et al[22] proposed the ADC-dependent vcDWI to improve the visibility of diffusion-restricted lesions in DWI. Based on formula (1), each voxel's ADC value was obtained from measured diffusion-weighted imaging (mDWI); the *b*-values b(x) are defined separately for each voxel position x, and SIs are computed at each voxel position x using formula (2). The dependency of the choice of b(x) on the voxel ADC values is established by a simple linear function[22]:

$$\beta(x) = k\ \ ADC(x)\ with\ k = 10^6 \frac{s^2}{mm^4} \quad (3)$$

Then, the voxel signal in vcDWI is computed by combining Eqs (2) and (3).

$$\mathrm{SvcDWI(x)} = \mathrm{S_0(x)}\ \exp(-\mathrm{k\ ADC(x^2)}\ \mathrm{with\ k} = 10^6 \frac{\mathrm{s^2}}{\mathrm{mm^4}}$$

Thereafter, the vcDWI map is generated. According to the vcDWI theory,[22] the voxels with low ADC (restricted-diffusion areas) are computed at a lower *b*-value, and the voxels with high ADC (nonrestricted-diffusion areas) are computed at a higher *b*-value.

Quantitative analysis of cDWI and vcDWI

The signal intensities were determined by drawing circular two-dimensional regions of interest (ROIs) on the DWI images. The ROIs were created with Image J (NIH, Bethesda, MD; https://imagej.nih.gov/ij/). Tumor ROIs were manually delineated freehand around the mass at the largest level of the tumor on cDWI (b = 1000 s/mm^2) image, and avoided necrotic, cystic, and hemorrhagic parts. T_2WI and DCE-MRI images were used to help locate the lesions and verify the lesion boundaries. The shape and size of the ROI was chosen to maximize the ROI size within the tumor while minimizing the partial volume effects. A similar-sized ROI was then placed in the normal gland parenchyma and the background tissue. The mean ROI area was 18 mm^2 (range 4–65 mm^2). In order to ensure the accuracy of the ROI drawing, all sets of ROIs were respectively drawn by two radiologists (WMH and ZJJ) with 18 and 9 years' of experience, respectively, who had knowledge of the histopathological findings and the clinical data. Two radiologists made a weekly comparison and discussion of the ROIs, and chose one set of ROIs if positions of the drawing were basically the same; if there was a great difference between the two radiologists, another senior radiologist would be involved to reach a consensus, and the ROI would be redrawn after the discussion. A set of ROIs were copied onto the same axial section of other DWI scans, but not mDWI scans. The ROIs in mDWI scans were drawn separately, as its direction was opposite to that of cDWI and vcDWI. In normal glandular tissue, ROIs were carefully chosen such that they were not near the lesion in the same breast (at least 2 cm from the index lesion) and avoided lipid. We measured the SI of the lesion, normal glandular tissue, and background noise on mDWI, cDWI, and vcDWI images. Then, the CRs between cancerous and non-cancerous lesions, and the SNRs were calculated. Each CR of breast cancer was calculated as CR = (S_{ca}-S_n) / (S_{ca} + S_n), while SNR was calculated as S_{ca} /N, where Sca indicated the SI for the malignant lesion and S_n meant SI for the normal glandular tissue; N denoted the standard deviation of background intensity.

Table 2. Compared SNR and CR in advanced processed DWI with mDWI

	SNR		CR	
	mean	p	mean	p
$cDWI_{1000}$	227.39	0.230	0.490	0.394
$cDWI_{1500}$	97.29	<0.001	0.550	0.006
$cDWI_{2000}$	46.59	<0.001	0.589	<0.001
$cDWI_{2500}$	23.79	<0.001	0.611	<0.001
$cDWI_{3000}$	12.63	<0.001	0.621	<0.001
$cDWI_{3500}$	6.89	<0.001	0.625	<0.001
$cDWI_{4000}$	3.85	<0.001	0.623	<0.001
vcDWI	166.64	0.189	0.663	<0.001
mDWI	212.57	-	0.440	-

CR, contrast ratio; SNR, signal-to-noise ratio; cDWI, computed diffusion-weighted imaging; mDWI, measured diffusion-weighted imaging; vcDWI, voxelwise computed diffusion-weighted imaging.

STATISTICAL ANALYSES

Data analysis was performed with SPSS v. 19.0 software (SPSS, Inc.; Chicago, IL, USA). Wilcoxon's signed-rank test was used to compare differences among the three different DWI techniques (mDWI, cDWI, and vcDWI) due to the non-normal distribution of the data. SNRs and CRs of the different types of post-processed DWI and conventional DWI were compared using the Wilcoxon test. Probability values of less than 0.05 were considered statistically significant.

RESULTS

CR comparisons

The mean values of SNR and CR are summarized in Table 2. vcDWI provided the best CR for the detection of breast cancer. The CRs of vcDWI and all cDWIs except $cDWI_{1000}$ differed significantly from that of mDWI. CR rose somewhat with increasing *b*-values, and reached a plateau; the increase in CR was not obvious, and $cDWI_{4000}$ even showed a slightly lower CR than did $cDWI_{3500}$ (Figure 1).

SNR COMPARISONS

Although the mean SNR of $cDWI_{1000}$ was slightly higher and the mean SNR of vcDWI was slightly lower than that of mDWI, the SNRs of $cDWI_{1000}$ and vcDWI did not differ significantly from that of mDWI (mDWI: SNRmean = 212.57; $cDWI_{1000}$: SNRmean = 227.89, p = 0.230; vcDWI: SNRmean = 166.64, p = 0.189). The SNRs of the remaining cDWIs all differed statistically significantly from that of mDWI, and the mean SNR of cDWI was significantly lower than that of mDWI ($cDWI_{1500}$: SNRmean

Figure 1. Mean value of the CR for breast cancer. vcDWI provided the best CR, while the value of CR increased with increasing *b*-values in cDWIs. (*$p < 0.05$, as compared to mDWI). cDWI, computed diffusion-weighted imaging; CR, contrast ratio; mDWI, measured diffusion-weighted imaging.

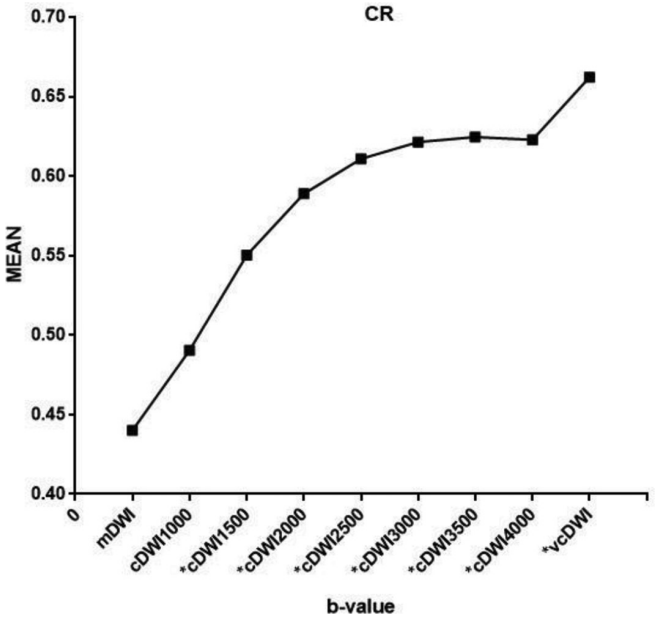

Figure 2. Mean SNR for each DWI. SNRmean of $cDWI_{1000}$ and vcDWI did not differ significantly from that of mDWI. In cDWIs, SNR decreased with increasing b-values, and the initial decrease at low b-values was steeper than the more gradual attenuation at higher b-values. (*$p < 0.05$ when compared to mDWI). cDWI, computed diffusion-weighted imaging; mDWI, measured diffusion-weighted imaging;SNR, signal-to-noise ratio; vcDWI, voxelwise computed diffusion-weighted imaging.

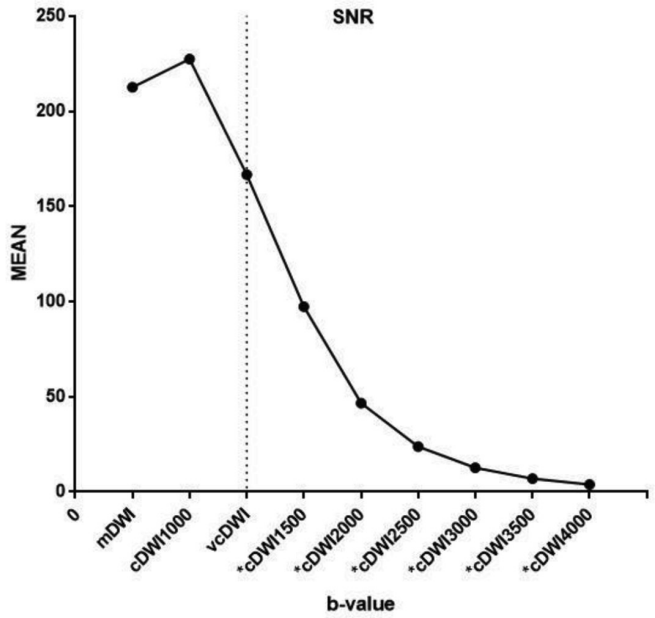

= 97.29, $p < 0.001$; $cDWI_{2000}$: SNRmean = 46.59, $p < 0.001$; $cDWI_{2500}$: SNRmean = 23.79, $p < 0.001$; $cDWI_{3000}$: SNRmean = 12.63, $p < 0.001$; $cDWI_{3500}$: SNRmean = 6.89, $p < 0.001$; $cDWI_{4000}$: SNRmean = 3.85, $p < 0.001$). For the set of cDWIs, the SNR declined with increasing *b*-values, and the initial decrease at low *b*-values was steeper than the more gradual attenuation seen at higher *b*-values (Figure 2).

Comprehensive comparison in cDWI

For a more comprehensive comparison of cDWI, all CR values were magnified by 100 times (CR_{100}), and then the CR_{100} and SNR values were plotted. In the graph, as *b*-values increased, the SNR declined, while CR_{100} gradually rose. These ratios converged at a *b*-value ranging from 1500 to 2000 s/mm^2 (Figure 3).

DISCUSSION

This study quantitatively evaluated the value of new DWI techniques (cDWI and vcDWI) in comparison with conventional DWI (mDWI) for detection of breast cancer, by investigating the CR or conspicuity of lesions, and the quality or SNR of the images, because these aspects markedly impact radiologists' assessment of scans. We found that vcDWI provided the best CR, as compared with mDWI or cDWIs(Figure 4 and Figure 5) , for the detection of breast cancer, and that *b*-values ranging from 1500 to 2000 s/mm^2 were optimal for detecting breast cancer on cDWI.

Figure 3. A plot of CR_{100} (the value of CR amplified 100 times) and SNR. With increasing *b*-values, SNR declined, while CR rose gradually. These two ratios converged at a b-value ranging from 1500 to 2000 s/mm^2. Computed *b*-values in the range of 1500–2000 s/mm^2 were optimal for breast cancer detection. cDWI, computed diffusion-weighted imaging; CR, contrast ratio;SNR, signal-to-noise ratio.

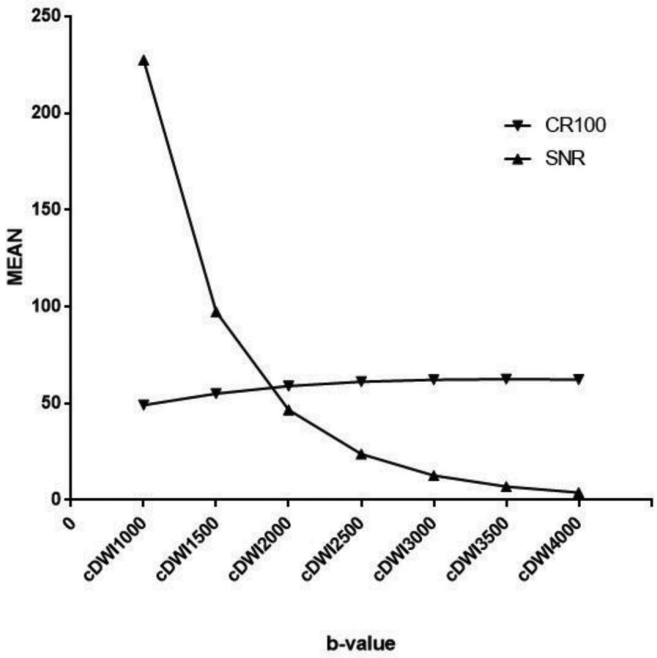

Figure 4. A 56-year-old female with a breast medullary carcinoma in the left lateral mammary. cDWI (a–g), vcDWI (h), mDWI (i). The lesion indicated extreme hyperintensity on vcDWI and cDWI with relatively lower *b*-values. With increasing *b*-values, image quality declined, and the lesion was not visible at $cDWI_{4000}$. cDWI, computed diffusion-weighted imaging; mDWI, measured diffusion-weighted imaging; vcDWI, voxelwise computed diffusion-weighted imaging.

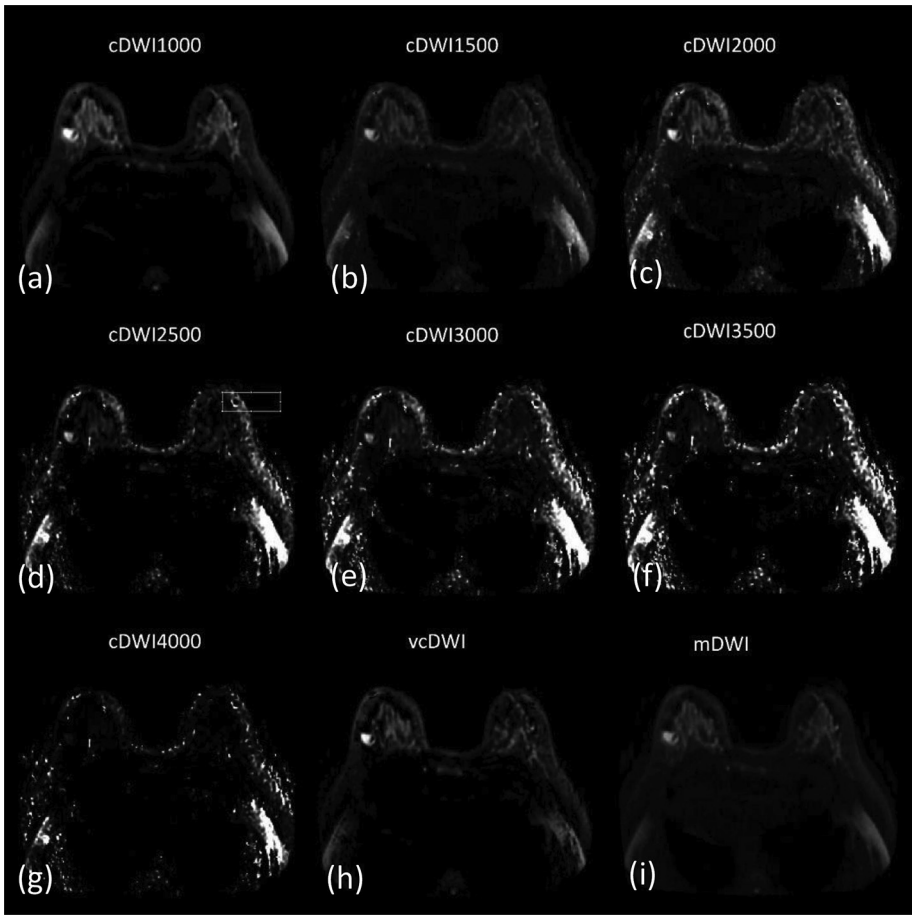

The lesion SI in DWI is affected by both diffusivity and T_2 relaxation of tissues. High SIs in DWI thus do not necessarily correspond to diffusion-restricted areas, but could also result from long tissue T_2 relaxation times (known as the T_2 shine-through effect), which complicates lesion identification[20]. Hence, the diagnosis of a lesion with high SI in DWI should be combined with T_2 weighted images or ADC maps to determine whether the region is truly diffusion-restricted. To avoid this in a clinical context, it is necessary to increase the *b*-value of the DWI protocol; although this can be achieved practically, it requires larger diffusion-sensitizing gradients and longer echo times, which may result in susceptibility to artifacts and severe eddy current distortions, as well as low SNRs and increased scanning time.

cDWI is a mathematical computation method that generates higher *b*-value DWI from images acquired with lower *b*-values, Blackledge et al[23] found that cDWI had improved contrast, without increasing scanning time, than initial lower *b*-value images, and improved SNR as compared with mDWI images obtained with the same high *b*-value. Although the CRs increased with the rise in *b*-values in a set of cDWIs, the SNR or image quality declined, although this decline was more gradual in cDWI than in mDWI. This may cause some small tumors or lesions to be missed, as Gatidis et al[22] reported for a patient with prostate cancer and multiple bone metastases, in whom a small bone metastasis was not detectable in the high *b*-value cDWI images, due to high image noise levels. On the whole, cDWI can provide a relatively better CR and detectability than mDWI, and has a better SNR than mDWI performed at the same high *b*-value.[17,19] Nevertheless, in this study, we did not use a high *b*-value DWI scanning protocol, and thus, we could not show whether cDWI could provide a better SNR or CR than mDWI at the same *b*-value.

In our study, we also found that, for cDWI, *b*-values ranging from 1500 to 2000 s/mm^2 were optimal for breast cancer detection. This differed somewhat from previous studies that reported that *b*-values ranging from 1500 to 2500 s/mm^2 were optimal for prostate cancer diagnosis;[21] the latter range was wider than that of the present study, and may be related to differences in subjects and anatomic sites.

We found that SNR declined with increasing *b*-values, which was consistent with the findings of Ueno et al, who reported that the initial decrease in SIs at low *b*-values was steeper than the

Figure 5. A 66-year-old female with an invasive ductal carcinoma in the deep center of the right mammary. cDWI (a–g), vcDWI (h), mDWI (i). The tumor was markedly more conspicuous on vcDWI and mDWI with a *b*-value 1000 mm/s^2, with a more distinct margin, than on other DWIs. The lesion gradually became unclear with increasing b-values in cDWI. cDWI, computed diffusion-weighted imaging; mDWI, measured diffusion-weighted imaging; vcDWI, voxelwise computed diffusion-weighted imaging.

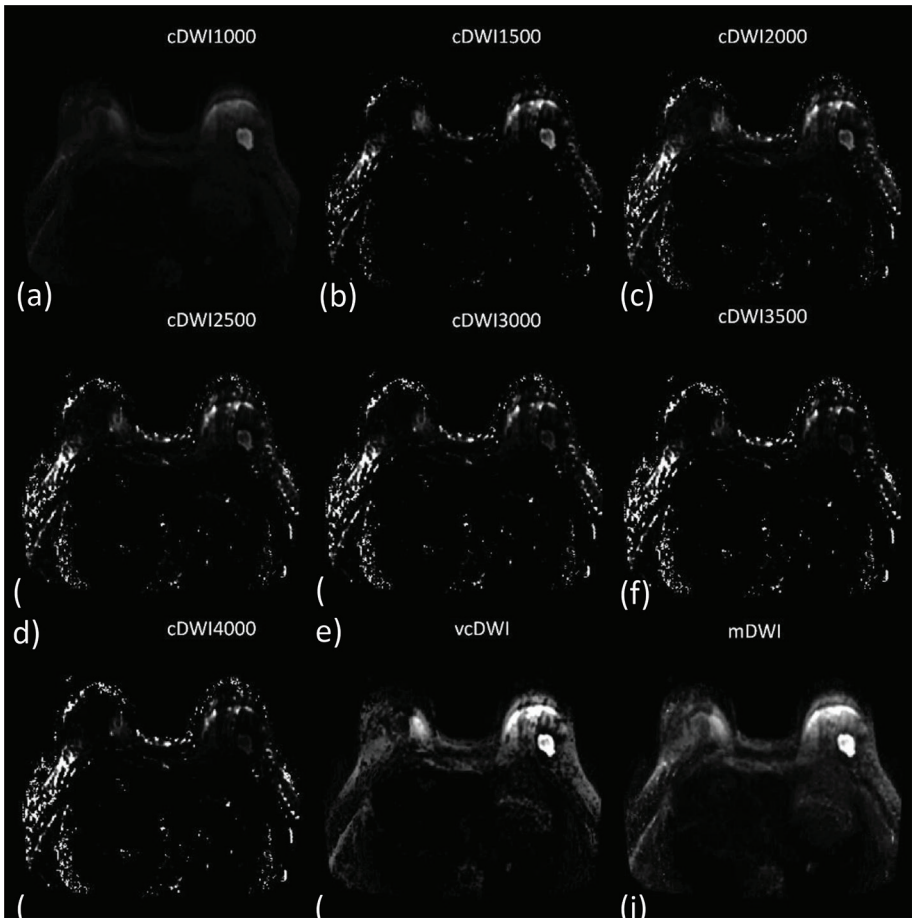

more gradual attenuation of SIs at higher *b*-values.[14] We only used several low *b*-values (600, 800, 1000 s/mm^2), and did not perform high *b*-value DWI.

vcDWI is based on the theory that SI reduction is mainly found in nonrestricted diffusion tissues, while SI is mainly preserved in diffusion-restricted tissues. Every local voxel involved a different high *b*-value, SIs of voxels with a low ADC were computed at a lower *b*-value to preserve voxel SNR, while voxels with a higher ADC were displayed at higher *b*-value to decrease the SI. Therefore, vcDWI could allow comparatively better detectability of tumor than mDWI, and preserved the SNR of the tumor relatively well, as compared to cDWI or mDWI with high *b*-values. vcDWI could also provide better SNR and maintain better CR without requiring additional scanning time. In the present study, vcDWI demonstrated the best ability for detecting malignant breast lesions by increasing the CR between the tumor and normal glandular tissue. It may allow more accurate diagnosis and better breast lesion detection in a clinical context.

Our study had several limitations. First, we did not use a unified *b*-value in the DWI protocol; different *b*-values were used (600, 800, 1000 s/mm^2) for breast examination, and the cDWIs were calculated using different combinations of *b*-values, which may impact the results slightly. Although some reports[14] have recommended $b \geq 10$ s/mm^2 and $b \geq 500$ s/mm^2, as well as $b = 0$ s/mm^2 and $b = 1000$ s/mm^2, specific combinations of *b*-values remain undefined. Second, our study made quantitative judgments of advanced DWI (cDWIs and vcDWI) of the breast lesion; all results were obtained by using an objective number or the trend of the correlated graph. Qualitative assessments, such as image quality, the degree of tumor malignancy, background signal suppression, and subjective conspicuity of the tumor were not evaluated in this study. Qualitative image analysis has to pursued in future studies. Third, the ROIs may have some impact on the results, as they were drawn separately in mDWI and cDWI. Fourth, our study does not take benign lesions into account. Finally, the patient population used was relatively small; larger prospective trials need to be performed.

CONCLUSION

We show that, for cDWI, a higher *b*-value is not necessarily better; in our study, *b*-values in the range of 1500 to –2000 s/mm^2 was optimal for detecting breast cancer. Furthermore, we demonstrate that ADC-dependent vcDWI provides the best DWI contrast optimization. It not only provides a better

CR between breast cancer and normal glandular tissue than does mDWI and cDWI, and also improves image quality, and is thus a promising approach for facilitating detection of breast cancer in a clinic context. It may simplify qualitative image analysis, rendering the comparison of multiple diffusion-weighted images or the ADC map unnecessary. The clinical impact on these advantages have to be evaluated in further studies.

REFERENCES

1. Stadlbauer A, Bernt R, Gruber S, Bogner W, Pinker K, van der Riet W, et al. Diffusion-weighted MR imaging with background body signal suppression (DWIBS) for the diagnosis of malignant and benign breast lesions. *Eur Radiol* 2009; **19**: 2349–56. doi: https://doi.org/10.1007/s00330-009-1426-2
2. O'Flynn EAM, Blackledge M, Collins D, Downey K, Doran S, Patel H, et al. Evaluating the diagnostic sensitivity of computed diffusion-weighted MR imaging in the detection of breast cancer. *J Magn Reson Imaging* 2016; **44**: 130–7. doi: https://doi.org/10.1002/jmri.25131
3. Padhani AR, Koh D-M, Collins DJ. Whole-body diffusion-weighted MR imaging in cancer: current status and research directions. *Radiology* 2011; **261**: 700–18. doi: https://doi.org/10.1148/radiol.11110474
4. Maas MC, Fütterer JJ, Scheenen TWJ. Quantitative evaluation of computed high B value diffusion-weighted magnetic resonance imaging of the prostate. *Invest Radiol* 2013; **48**: 779–86. doi: https://doi.org/10.1097/RLI.0b013e31829705bb
5. Padhani AR, Liu G, Koh DM, Chenevert TL, Thoeny HC, Takahara T, et al. Diffusion-weighted magnetic resonance imaging as a cancer biomarker: consensus and recommendations. *Neoplasia* 2009; **11**: 102–25. doi: https://doi.org/10.1593/neo.81328
6. Marini C, Iacconi C, Giannelli M, Cilotti A, Moretti M, Bartolozzi C. Quantitative diffusion-weighted MR imaging in the differential diagnosis of breast lesion. *Eur Radiol* 2007; **17**: 2646–55. doi: https://doi.org/10.1007/s00330-007-0621-2
7. Taplin SH, Rutter CM, Elmore JG, Seger D, White D, Brenner RJ. Accuracy of screening mammography using single versus independent double interpretation. *AJR Am J Roentgenol* 2000; **174**: 1257–62. doi: https://doi.org/10.2214/ajr.174.5.1741257
8. Maas MC, Fütterer JJ, Scheenen TWJ. Quantitative evaluation of computed high B value diffusion-weighted magnetic resonance imaging of the prostate. *Invest Radiol* 2013; **48**: 779–86. doi: https://doi.org/10.1097/RLI.0b013e31829705bb
9. Tanimoto A, Nakashima J, Kohno H, Shinmoto H, Kuribayashi S. Prostate cancer screening: the clinical value of diffusion-weighted imaging and dynamic MR imaging in combination with T2-weighted imaging. *J Magn Reson Imaging* 2007; **25**: 146–52. doi: https://doi.org/10.1002/jmri.20793
10. Mardor Y, Roth Y, Ochershvilli A, Spiegelmann R, Tichler T, Daniels D, et al. Pretreatment prediction of brain tumors' response to radiation therapy using high b-value diffusion-weighted MRI. *Neoplasia* 2004; **6**: 136–42. doi: https://doi.org/10.1593/neo.03349
11. Rosenkrantz AB, Chandarana H, Hindman N, Deng F-M, Babb JS, Taneja SS, et al. Computed diffusion-weighted imaging of the Prostate at 3 T: impact on image quality and tumour detection. *Eur Radiol* 2013; **23**: 3170–7. doi: https://doi.org/10.1007/s00330-013-2917-8
12. Ueno Y, Takahashi S, Ohno Y, Kitajima K, Yui M, Kassai Y, et al. Computed diffusion-weighted MRI for prostate cancer detection: the influence of the combinations of b-values. *Br J Radiol* 2015; **88**: 20140738. doi: https://doi.org/10.1259/bjr.20140738
13. Ueno Y, Takahashi S, Kitajima K, Kimura T, Aoki I, Kawakami F, et al. Computed diffusion-weighted imaging using 3-T magnetic resonance imaging for prostate cancer diagnosis. *Eur Radiol* 2013; **23**: 3509–16. doi: https://doi.org/10.1007/s00330-013-2958-z
14. Feuerlein S, Davenport MS, Krishnaraj A, Merkle EM, Gupta RT. Computed high b-value diffusion-weighted imaging improves lesion contrast and conspicuity in prostate cancer. *Prostate Cancer Prostatic Dis* 2015; **18**: 155–60. doi: https://doi.org/10.1038/pcan.2015.5
15. Moribata Y, Kido A, Fujimoto K, Himoto Y, Kurata Y, Shitano F, et al. Feasibility of computed diffusion weighted imaging and optimization of b-value in cervical cancer. *Magn Reson Med Sci* 2017; **16**: 66–72. doi: https://doi.org/10.2463/mrms.mp.2015-0161
16. Gatidis S, Schmidt H, Martirosian P, Nikolaou K, Schwenzer NF. Apparent diffusion coefficient-dependent voxelwise computed diffusion-weighted imaging: an approach for improving SNR and reducing T2 shine-through effects. *J Magn Reson Imaging* 2016; **43**: 824–32. doi: https://doi.org/10.1002/jmri.25044
17. Ichikawa T, Erturk SM, Motosugi U, Sou H, Iino H, Araki T, et al. High-b value diffusion-weighted MRI for detecting pancreatic adenocarcinoma: preliminary results. *AJR Am J Roentgenol* 2007; **188**: 409–14. doi: https://doi.org/10.2214/AJR.05.1918
18. Maas MC, Fütterer JJ, Scheenen TWJ. Quantitative evaluation of computed high B value diffusion-weighted magnetic resonance imaging of the prostate. *Invest Radiol* 2013; **48**: 779–86. doi: https://doi.org/10.1097/RLI.0b013e31829705bb
19. Rosenkrantz AB, Chandarana H, Hindman N, Deng F-M, Babb JS, Taneja SS, et al. Computed diffusion-weighted imaging of the Prostate at 3 T: impact on image quality and tumour detection. *Eur Radiol* 2013; **23**: 3170–7. doi: https://doi.org/10.1007/s00330-013-2917-8
20. Colagrande S, Belli G, Politi LS, Mannelli L, Pasquinelli F, Villari N. The influence of diffusion- and relaxation-related factors on signal intensity: an introductive guide to magnetic resonance diffusion-weighted imaging studies. *J Comput Assist Tomogr* 2008; **32**: 463–74. doi: https://doi.org/10.1097/RCT.0b013e31811ec6d4
21. Rosenkrantz AB, Parikh N, Kierans AS, Kong MX, Babb JS, Taneja SS, et al. Prostate cancer detection using computed very high b-value diffusion-weighted imaging: how high should we go? *Acad Radiol* 2016; **23**: 704–11. doi: https://doi.org/10.1016/j.acra.2016.02.003
22. Cornfeld DM, Israel G, McCarthy SM, Weinreb JC. Pelvic imaging using a T1W fat-suppressed three-dimensional dual echo Dixon technique at 3T. *J Magn Reson Imaging* 2008; **28**: 121–7. doi: https://doi.org/10.1002/jmri.21402
23. Blackledge MD, Leach MO, Collins DJ, Koh D-M. Computed diffusion-weighted MR imaging may i mprove tumor detection. *Radiology* 2011; **261**: 573–81. doi: https://doi.org/10.1148/radiol.11101919